JOURNAL OF COMPUTATIONAL PHYSICS 108, 236-245 (1993)

Analysis of Three-Dimensional Electromagnetic Fields Using Edge Elements

R. ALBANESE

Dipartimento di Ingegneria Elettronica, Università di Salerno, Via Ponte Don Melillo, I-84084 Fisciano (SA), Italy

AND

G. RUBINACCI

Dipartimento di Ingegneria Industriale, Università degli Studi di Cassino, Via Zamosch 43, I-03403 Cassino, Italy

Received November 20, 1992; accepted February 9, 1993

Dual formulations of the three-dimensional magnetostatic and eddy current problems in terms of two-component vector potentials are described. Cancellation errors and interface problems are avoided by means of a numerical procedure based on the adoption of edge elements. The numerical approaches are characterised by a unified treatment of magnetostatic and eddy current problems. Each of the two formulations enforces one of the two canonical field equations exactly. In this way, taking the solution (**E**, **B**) which results from the electric formulation and the solution (**H**, **J**) coming out from the magnetic one, the numerical error is concentrated on the constitutive equations. This allows for an estimation of the global error and provides a useful indication for the mesh refinements. The possibility of determining upper and lower bounds for power/energy related parameters, well known in the magnetostatic case, is also discussed for the eddy current problem.

INTRODUCTION

Complementary solutions provide a useful theoretical basis for the development of several computational methods in engineering. These formulations give the possibility to determine upper and lower bounds or power/energy related parameters and to estimate the errors of the approximate solutions.

In the context of computational magnetostatics, complementary solutions can be found by enforcing the canonical equations $\nabla \cdot \mathbf{B} = 0$ and $\nabla \times \mathbf{H} = \mathbf{J}_s$ and minimising a functional $A(\mathbf{B}, \mathbf{H})$ which is related to the error on the constitutive equation $\mathbf{B} = \mathbf{B}(\mathbf{H})$, and is zero if evaluated at the correct solution $\mathbf{B} = \mathbf{B}_0$, $\mathbf{H} = \mathbf{H}_0$ [1]. The error functional can be split into the sum of two different functionals $\Xi(\mathbf{B})$ and $\Theta(\mathbf{H})$, thus providing two different formulations in **B** and **H**, and giving the possibility to define upper and lower bounds for the quantity $\Theta(\mathbf{H}_0) = -\Xi(\mathbf{B}_0)$, which is related to the magnetic energy of the system.

Dual formulations have been discussed for transient and steady state eddy current problems [2–5]. However, in these cases, well defined bounds for power or energy functionals have not been clearly established [2].

In any case, the use of formulations that exactly verify the canonical field equations provides a powerful tool for the error estimation. In fact, in this case, the error is concentrated in the constitutive equations and can directly be measured. This provides a useful indication for the mesh refinement, to be especially performed where the pairs (**B**, **H**) or (**J**, **E**) are far from satisfying the constitutive equations.

Enforcing the canonical equations in three dimensional geometry can readily be achieved by choosing numerical formulations based on the use of two-component vector potentials and the adoption of edge elements [6–8].

In this paper we will describe the three-dimensional magnetostatic and eddy current problems in terms of two-component vector potentials using edge elements. On the basis of numerical results and theoretical considerations, we discuss the possibility of defining upper and lower bounds for power/energy related functionals for the eddy current problem too.

BASIC EQUATIONS

The Magnetostatic Problem

We refer to the magnetostatic problem in a bounded region V described by the field equations

$$\nabla \times \mathbf{H} = \mathbf{J}_s \quad \text{in } V \tag{1}$$

$$\nabla \cdot \mathbf{B} = 0 \quad \text{in } V, \tag{2}$$

0021-9991/93 $5.00

the consitutive equation,

$$\mathbf{B} = \mathbf{B}(\mathbf{H}) \quad \text{in } V, \tag{3}$$

and suitable boundary conditions like $\mathbf{B} \cdot \mathbf{n} = b$ on $\partial V_b \subseteq \partial V$ and $\mathbf{H} \times \mathbf{n} = \mathbf{h}$ on $\partial V_h \subseteq \partial V$.

Here $\mathbf{B}$ is the magnetic induction, $\mathbf{H}$ is the field intensity, $\mathbf{J}_s$ is an externally imposed current density distribution, and b and $\mathbf{h}$ are prescribed values on the boundary. The constitutive operator (3) is supposed to be continuous, symmetric and monotone, so that Eq. (3) can also be replaced by $\mathbf{H} = \mathbf{H}(\mathbf{B})$.

The Eddy Current Problem

We assume the mathematical model defined by the field equations:

$$\nabla \times \mathbf{H} = \mathbf{J} \qquad \text{in } V \tag{4}$$

$$\nabla \times \mathbf{E} = -\frac{\partial \mathbf{B}}{\partial t} \quad \text{in } V, \tag{5}$$

the linear material properties

$$\mathbf{B} = \mu \mathbf{H} \qquad \text{in } V \tag{6}$$

$$\mathbf{J} = \sigma \mathbf{E} + \mathbf{J}_s \quad \text{in } V, \tag{7}$$

initial conditions verifying $\nabla \cdot \mathbf{B} = 0$, and suitable boundary conditions like $\mathbf{E} \times \mathbf{n} = \mathbf{e}$ on $\partial V_e \subseteq \partial V$ or $\mathbf{H} \times \mathbf{n} = \mathbf{h}$ on $\partial V_h \subseteq \partial V$. Here $\mathbf{E}$ is the electric field, t is the time, μ is the magnetic permeability, σ is the electric conductivity (non-zero only in the conducting region V_c), and $\mathbf{e}$ or $\mathbf{h}$ are specified values on the boundary.

These equations determine the magnetic field distribution in V, along with current density and electric field in V_c. Note that in this model, in which the displacement current is neglected, the electric field is not uniquely determined in the external region $V - V_c$. A way to have the uniqueness of $\mathbf{E}$ in the external region is to specify its divergence (related to the charge distribution) in $V - V_c$.

TWO-COMPONENT VECTOR POTENTIALS AND EDGE ELEMENTS

All the electromagnetic quantities ($\mathbf{B}$, $\mathbf{H}$, $\mathbf{E}$ and $\mathbf{J}$) can be discontinuous at magnetic or electric interfaces. Therefore, in these cases, they can hardly be expanded in terms of continuous functions. There are two possible ways of overcoming this problem without introducing double-valued functions at the discontinuity interfaces.

The first approach falls within the framework of the finite element methods and is based on the use of a particular set of vector shape functions, for which the continuity of the tangential components is preserved, allowing for the discontinuity of the normal component between adjacent elements. Such features can be obtained by using the edge elements, introduced in [9–10] and generalised in [11–14], whose degrees of freedom are associated with the tangential components (or the line integrals) of the vector field along the edges. A shape function in a hexahedral edge element is illustrated with its curl in Fig. 1. Field formulations using edge elements have been proposed and applied in terms of $\mathbf{E}$ or $\mathbf{H}$ [15, 16].

The second approach is based on the introduction of vector and scalar potentials in conjunction with the Coulomb or Lorentz gauges [17–19], expressing the field intensity as $\mathbf{H} = \mathbf{T} - \nabla\Omega$ ($\mathbf{T}$ is the electric vector potential) or the electric field as $\mathbf{E} = -\partial\mathbf{A}/\partial t - \nabla\partial\phi/\partial t$ ($\mathbf{A}$ is the magnetic vector potential). In this way, at the magnetic interfaces, the possible jump of the normal component of $\mathbf{H}$ is absorbed by a discontinuity of $\partial\Omega/\partial n$, and both Ω and the three components of $\mathbf{T}$ can be kept continuous. The same happens for the electric field at the electric interfaces. The price to be paid using this approach is the introduction of an additional scalar unknown (the scalar potential), which unavoidably gives rise to another equation.

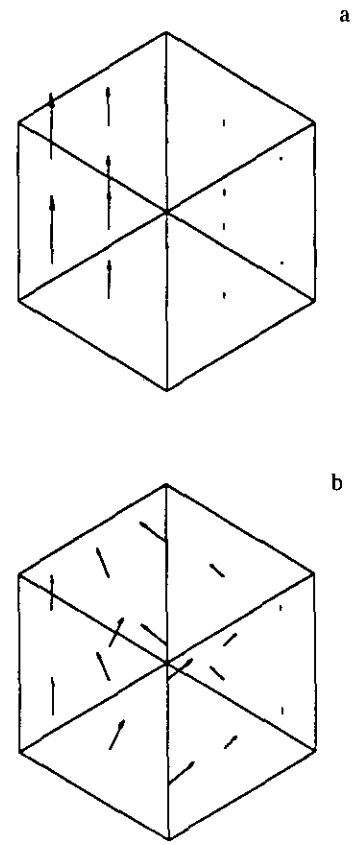

FIG. 1. Shape function $\mathbf{N}_k$ (a) and its curl $\nabla \times \mathbf{N}_k$ (b) in the master element.

The total number of scalar unknowns is brought back to three by adopting the gauge conditions:

$$\mathbf{T} \cdot \mathbf{w} = 0 \tag{8}$$

$$\mathbf{A} \cdot \mathbf{w} = 0 \tag{9}$$

with $\mathbf{w}$ selected as an arbitrary vector field without closed field lines. This approach was first used in conjunction with isoparametric elements, so postulating the continuity of the two nonzero components of the vector potentials [20–22]. However, the discontinuity interfaces, including the boundary of the conducting regions, were not taken into account adequately. In addition, with reference to the $\mathbf{T}, \Omega$ method, it was difficult to confine the electric vector potential inside the conducting regions, and large numerical errors arose in the magnetic regions (where $\mathbf{H}$ is small when compared to $\mathbf{T}$ and $\nabla\Omega$ separately).

All these problems were overcome by using edge-elements based shape functions $\mathbf{N}_k$ to approximate the vector potentials, standard isoparametric shape functions φ_k for the scalar potentials, and a numerical way of imposing gauge conditions (8)–(9) [7, 8]. With reference to the graph made up of nodes and edges of the edge-element mesh, the discrete analogue of conditions (8)–(9) was obtained by identifying the direction of $\mathbf{w}$ along an arbitrary tree of the graph, so connecting all the nodes without forming closed loops. The degrees of freedom corresponding to the edges of the tree were eliminated, and the remaining degrees of freedom were thus related to the fluxes of $\mathbf{J} = \nabla \times \mathbf{T}$ or $\mathbf{B} = \nabla \times \mathbf{A}$ linked with the set of independent loops closed by adding each of the residual edges (i.e., each edge of the co-tree) to the tree [7, 8]. This technique can readily be interpreted in analogy with basic circuit theory and is also the discrete analogue of the gauge $\mathbf{T} \cdot \mathbf{w} = 0$, where the field lines of $\mathbf{w}$ are given by the edges of the tree. This method was applied to both integral and differential formulations of electromagnetic problems.

The integral formulation of the three-dimensional eddy current problem in nonmagnetic media, presented in [7] and based on the two-component electric vector potential, is extremely powerful to analyse the eddy currents induced in both massive conductors and thin shells. In massive structures, the scalar degrees of freedom are only two, because the calculation of the scalar potential is not strictly required. On the other hand, the method naturally reduces to the stream function approach when applied to thin shells [23].

Inside the conducting regions, the differential formulations in terms of two-component electric and magnetic vector potentials $\mathbf{T}$ and $\mathbf{A}$ are practically equivalent to the edge-element-based eddy current approaches in terms of $\mathbf{H}$ and $\mathbf{E}$, respectively. The difference is in the unified treatment of conducting and nonconducting regions and of magnetostatic and eddy current problems.

DUAL FORMULATIONS OF THE MAGNETOSTATIC PROBLEM

To assume that the error is concentrated in the constitutive Eq. (3), it is indispensable to guarantee that the canonical Eqs. (1)–(2) are satisfied. This can be ensured by assuming $\mathbf{B} = \nabla \times \mathbf{A}$ and $\mathbf{H} = \mathbf{T}\text{-}\nabla\Omega$, with the two-component vector potentials approximated as described in the previous section.

In this way, Eq. (2) is automatically implied. As far as Eq. (1) is concerned, it is satisfied, provided that $\mathbf{T}$ is selected such as to verify

$$\nabla \times \mathbf{T} = \mathbf{J}_s. \tag{10}$$

This can be achieved by direct integration along the direction $\mathbf{w}$, or by approximating $\mathbf{T}$ as $\Sigma c_k \mathbf{N}_k$ and applying the weak formulation

$$\int_V \nabla \times \mathbf{N}_k \cdot \nabla \times \mathbf{T}\, dV = \int_V \nabla \times \mathbf{N}_k \cdot \mathbf{J}_s\, dV \quad \forall \mathbf{N}_k \tag{11}$$

which is equivalent to minimising the error functional

$$\Phi(\mathbf{T}) = \tfrac{1}{2} \int_V (\nabla \times \mathbf{T} - \mathbf{J}_s)^2\, dV. \tag{12}$$

Thus, the problem of determining $\mathbf{B}$ and $\mathbf{H}$ is reduced to finding the best estimates of $\mathbf{A}$ and Ω.

Here we briefly recall the main points of the error based approach to complementary formulations of magnetostatic field solutions, presented in [1] and applied with the two-component vector potential in [8]. As shown in [1], the starting point is the definition of the local error density (for soft magnetic materials)

$$\lambda(\mathbf{B}, \mathbf{H}) = \int_0^{\mathbf{H}} \mathbf{B}(\mathbf{H}') \cdot d\mathbf{H}' + \int_0^{\mathbf{B}} \mathbf{H}(\mathbf{B}') \cdot d\mathbf{B}' - \mathbf{B} \cdot \mathbf{H} \geq 0 \tag{13}$$

which is zero only if the field estimates $\mathbf{B}$ and $\mathbf{H}$ satisfy the constitutive relationship (3). Note that, for linear media, i.e., if the constitutive equation is given by Eq. (6), the expression of the local error density becomes

$$\lambda(\mathbf{B}, \mathbf{H}) = (\mathbf{B} - \mu\mathbf{H})^2/2\mu = B^2/2\mu + \mu H^2/2 - \mathbf{B} \cdot \mathbf{H} \geq 0. \tag{14}$$

This allows for the definition of a global error functional

$$\Lambda(\mathbf{A}, \Omega) = \int_V \lambda(\nabla \times \mathbf{A}, \mathbf{T} - \nabla\Omega)\, dV = \Xi_v(\mathbf{A}) + \Theta_v(\Omega) + \Gamma(\mathbf{A}, \Omega) \geq 0, \tag{15}$$

where

$$\Xi_v(\mathbf{A}) = \int_V \left\{ \int_0^{\nabla \times \mathbf{A}} \mathbf{H}(\mathbf{B}) \cdot d\mathbf{B} \right\} dV \tag{16}$$

$$\Theta_v(\Omega) = \int_V \left\{ \int_0^{\mathbf{T} - \nabla\Omega} \mathbf{B}(\mathbf{H}) \cdot d\mathbf{H} \right\} dV \tag{17}$$

$$\Gamma(\mathbf{A}, \Omega) = -\int_V \nabla \times \mathbf{A} \cdot (\mathbf{T} - \nabla\Omega)\, dV. \tag{18}$$

If $\mathbf{A}$ and Ω are selected such as to verify the essential boundary conditions $\nabla \times \mathbf{A} \cdot \mathbf{n} = b$ on ∂V_b and $(\mathbf{T} - \nabla\Omega) \times \mathbf{n} = \mathbf{h}$ on ∂V_h [1, 8, 24], then $\Gamma(\mathbf{A}, \Omega)$ can be written as

$$\Gamma(\mathbf{A}, \Omega) = -\int_V \mathbf{A} \cdot \mathbf{J}_s\, dV - \int_{\partial V_h} \mathbf{A} \cdot \mathbf{h}\, dS + \int_{\partial V_b} \Omega b\, dS \tag{19}$$

and the error functional can be split into two separate contributions

$$\Lambda(\mathbf{A}, \Omega) = \Xi(\mathbf{A}) + \Theta(\Omega) \geqslant 0 \tag{20}$$

with

$$\Xi(\mathbf{A}) = \int_V \left\{ \int_0^{\nabla \times \mathbf{A}} \mathbf{H}(\mathbf{B}) \cdot d\mathbf{B} - \mathbf{J}_s \cdot \mathbf{A} \right\} dV - \int_{\partial V_h} \mathbf{A} \cdot \mathbf{h}\, dS \tag{21}$$

$$\Theta(\Omega) = \int_V \left\{ \int_0^{\mathbf{T} - \nabla\Omega} \mathbf{B}(\mathbf{H}) \cdot d\mathbf{H} \right\} dV - \int_{\partial V_b} \Omega b\, dS. \tag{22}$$

Minimisation of $\Xi(\mathbf{A})$ yields

$$\int_V \nabla \times \mathbf{N}_k \cdot \mu^{-1} \nabla \times \mathbf{A}\, dV = \int_V \mathbf{N}_k \cdot \mathbf{J}_s\, dV + \int_{\partial V_h} \mathbf{N}_k \cdot \mathbf{h}\, dS \quad \forall \mathbf{N}_k, \tag{23}$$

whereas minimisation of $\Theta(\Omega)$ provides

$$\int_V \nabla \varphi_k \cdot \mu(\mathbf{T} - \nabla\Omega)\, dV = \int_{\partial V_b} \varphi_k b\, dS \quad \forall \varphi_k. \tag{24}$$

A visualisation of the local error density distribution can be obtained by reporting the cloud of pairs ($\mathbf{B} = \nabla \times \mathbf{A}$, $\mathbf{H} = \mathbf{T} - \nabla\Omega$) in a $B - H$ plane in comparison with the B – H curve representing the constitutive equation. We can calculate both local error λ and global error Λ, because both $\mathbf{B}$ and $\mathbf{H}$ are available on the same mesh. Of course, the local error distributions offer a clear indication for a mesh refinement, because $\lambda = 0$ is a necessary condition to have both $\mathbf{B} = \mathbf{B}_0$ and $\mathbf{H} = \mathbf{H}_0$.

In addition, there is the possibility of having energy bounds. If we call $\mathbf{A}_0$ and Ω_0 the exact solutions for $\mathbf{A}$ and Ω, respectively, then we have well-defined upper and lower bounds for the energy related quantity $\Theta(\Omega_0) = -\Xi(\mathbf{A}_0)$, according to the inequalities

$$\Theta(\Omega) \geqslant \Theta(\Omega_0) = -\Xi(\mathbf{A}_0) \geqslant -\Xi(\mathbf{A}) \quad \forall \Omega, \mathbf{A}. \tag{25}$$

These bounds can be used to give a useful estimate of the relative error ε_r in terms of energy functional: $\varepsilon_r \leqslant [\Theta(\Omega) + \Xi(\mathbf{A})]/\min[|\Xi(\mathbf{A})|, |\Theta(\Omega)|]$.

DUAL FORMULATIONS OF THE EDDY CURRENT PROBLEM

To assume that the error is concentrated in the constitutive Eqs. (6)–(7), it is necessary to enforce the canonical Eqs. (4)–(5) exactly. This can be done by assuming

$$\mathbf{E} = -\partial \mathbf{A}/\partial t - \nabla\, \partial\phi/\partial t \quad \text{(and therefore } \mathbf{B} = \nabla \times \mathbf{A}\text{)} \tag{26}$$

$$\mathbf{H} = \mathbf{T} - \nabla\Omega + \mathbf{T}_s \quad \text{(and therefore } \mathbf{J} = \nabla \times \mathbf{T} + \mathbf{J}_s\text{)}, \tag{27}$$

where scalar and two-component vector potentials are expanded as described before, and $\mathbf{J}_s$ is approximated by $\nabla \times \mathbf{T}_s$ using, for instance, Eq. (11).

In this case, two local errors can be defined, with reference to the two constitutive equations (6)–(7). A direct approach based on the local and time varying constitution errors was proposed in [2], where it is shown how it is impossible to split the error functional into the sum of two contributions depending on $\mathbf{E}$ and $\mathbf{H}$ separately.

However, the splitting can be achieved by making use of the Laplace transforms. Assuming $V = V_c$ and zero initial conditions for the sake of simplicity, we can define

$$\lambda_m(\hat{\mathbf{B}}, \hat{\mathbf{H}}, p) = \frac{(\hat{\mathbf{B}} - \mu\hat{\mathbf{H}})^2}{2\mu} = \frac{\hat{\mathbf{B}}^2}{2\mu} + \frac{\mu\hat{\mathbf{H}}^2}{2} - \hat{\mathbf{B}} \cdot \hat{\mathbf{H}} \tag{28}$$

$$\lambda_e(\hat{\mathbf{J}}, \hat{\mathbf{E}}, p) = \frac{(\hat{\mathbf{J}} - \sigma\hat{\mathbf{E}} - \hat{\mathbf{J}}_s)^2}{2\sigma p} = \frac{(\hat{\mathbf{J}} - \hat{\mathbf{J}}_s)^2}{2\sigma p} + \frac{\sigma\hat{\mathbf{E}}^2}{2p} - \frac{\hat{\mathbf{E}} \cdot (\hat{\mathbf{J}} - \hat{\mathbf{J}}_s)}{p}, \tag{29}$$

where p is the complex variable and $\hat{X}$ denotes the Laplace transform of $X(t)$.

Both complex quantities λ_m and λ_e are zero if and only if the field estimates verify the constitutive properties, and they assume real and positive values if p is real and positive.

From now on we shall assume p as a real positive quantity. In this case we can also define the global error functional

$$\begin{aligned}
&\Lambda(\hat{\mathbf{A}}+\nabla\hat{\phi},\ \hat{\mathbf{T}}-\nabla\hat{\Omega},\ p)\\
&\quad=\int_V \{\lambda_m(\nabla\times\hat{\mathbf{A}},\ \hat{\mathbf{T}}-\nabla\hat{\Omega}+\hat{\mathbf{T}}_s,\ p)\\
&\qquad+\lambda_e(\nabla\times\hat{\mathbf{T}}+\mathbf{J}_s,\ -p\hat{\mathbf{A}}-p\nabla\hat{\phi},\ p)\}\,dV\\
&\quad=\Xi_v(\hat{\mathbf{A}}+\nabla\hat{\phi},\ p)+\Theta_v(\hat{\mathbf{T}}-\nabla\hat{\Omega},\ p)\\
&\qquad+\Gamma(\hat{\mathbf{A}}+\nabla\hat{\phi},\ \hat{\mathbf{T}}-\nabla\hat{\Omega},\ p)\geqslant 0\\
&\qquad\qquad\forall \text{ real and positive } p,
\end{aligned}\tag{30}$$

where

$$\Xi_v(\hat{\mathbf{A}}+\nabla\hat{\phi},\ p)=\int_V\left\{\frac{(\nabla\times\hat{\mathbf{A}})^2}{2\mu}+\frac{\sigma p(\hat{\mathbf{A}}+\nabla\hat{\phi})^2}{2}-(\hat{\mathbf{A}}+\nabla\hat{\phi})\cdot\hat{\mathbf{J}}_s\right\}dV \tag{31}$$

$$\Theta_v(\hat{\mathbf{T}}-\nabla\hat{\Omega},\ p)=\int_V\left\{\frac{\mu(\hat{\mathbf{T}}-\nabla\hat{\Omega}+\hat{\mathbf{T}}_s)^2}{2}+\frac{(\nabla\times\hat{\mathbf{T}})^2}{2\sigma p}\right\}dV \tag{32}$$

$$\Gamma(\hat{\mathbf{A}}+\nabla\hat{\phi},\ \hat{\mathbf{T}}-\nabla\hat{\Omega},\ p)=-\int_V\nabla\cdot(\hat{\mathbf{A}}+\nabla\hat{\phi})\times(\hat{\mathbf{T}}-\nabla\hat{\Omega}+\hat{\mathbf{T}}_s)\,dV. \tag{33}$$

If the potentials are selected such as to verify the essential boundary conditions $(\mathbf{A}+\nabla\phi)\times\mathbf{n}=-\int\mathbf{e}\,dt$ on ∂V_e and $(\mathbf{T}-\nabla\Omega+\mathbf{T}_s)\times\mathbf{n}=\mathbf{h}$ on ∂V_h, then Γ can be written as

$$\Gamma(\hat{\mathbf{A}}+\nabla\hat{\phi},\ \hat{\mathbf{T}}-\nabla\hat{\Omega},\ p)=-\int_{\partial V_h}(\hat{\mathbf{A}}+\nabla\hat{\phi})\cdot\hat{\mathbf{h}}\,dS-\int_{\partial V_e}\frac{(\hat{\mathbf{T}}-\nabla\hat{\Omega}+\hat{\mathbf{T}}_s)\cdot\hat{\mathbf{e}}}{p}\,dS \tag{34}$$

and the error functional can be split into two separate contributions

$$\begin{aligned}
&\Lambda(\hat{\mathbf{A}}+\nabla\hat{\phi},\ \hat{\mathbf{T}}-\nabla\hat{\Omega},\ p)\\
&\quad=\Xi(\hat{\mathbf{A}}+\nabla\hat{\phi},\ p)+\Theta(\hat{\mathbf{T}}-\nabla\hat{\Omega},\ p)\geqslant 0,\\
&\qquad\forall \text{ real and positive } p
\end{aligned}\tag{35}$$

with

$$\Xi(\mathbf{A}+\nabla\hat{\phi},\ p)=\Xi_v(\hat{\mathbf{A}}+\nabla\hat{\phi},\ p)-\int_{\partial V_h}(\hat{\mathbf{A}}+\nabla\hat{\phi})\cdot\hat{\mathbf{h}}\,dS \tag{36}$$

$$\Theta(\hat{\mathbf{T}}-\nabla\hat{\Omega},\ p)=\Theta_v(\hat{\mathbf{T}}-\nabla\hat{\Omega},\ p)-\int_{\partial V_e}\frac{(\hat{\mathbf{T}}-\nabla\hat{\Omega}+\hat{\mathbf{T}}_s)\cdot\hat{\mathbf{e}}}{p}\,dS. \tag{37}$$

The stationary point of Ξ (as well as its minimisation for real and positive values of p) is given by

$$\int_V\{\nabla\times\mathbf{N}_k\cdot\mu^{-1}\nabla\times\hat{\mathbf{A}}+\mathbf{N}_k\cdot\sigma p(\hat{\mathbf{A}}+\nabla\hat{\phi})\}\,dV=\int_V\mathbf{N}_k\cdot\hat{\mathbf{J}}_s\,dV+\int_{\partial V_h}\mathbf{N}_k\cdot\hat{\mathbf{h}}\,dS,\quad\forall\mathbf{N}_k \tag{38}$$

$$\int_V\nabla\phi_k\cdot\sigma p(\hat{\mathbf{A}}+\nabla\hat{\phi})\,dV=\int_V\nabla\varphi_k\cdot\hat{\mathbf{J}}_s\,dV+\int_{\partial V_h}\nabla\varphi_k\cdot\hat{\mathbf{h}}\,dS,\quad\forall\varphi_k. \tag{39}$$

Similarly, the stationary point (minimum for $p\geqslant 0$) of Θ is given by

$$\int_V\{\nabla\times\mathbf{N}_k\cdot\sigma^{-1}\nabla\times\hat{\mathbf{T}}+\mathbf{N}_k\cdot\mu p(\hat{\mathbf{T}}-\nabla\Omega+\hat{\mathbf{T}}_s)\}\,dV=\int_{\partial V_e}\mathbf{N}_k\cdot\hat{\mathbf{e}}\,dS,\quad\forall\mathbf{N}_k \tag{40}$$

$$\int_V-\nabla\varphi_k\cdot\mu p(\hat{\mathbf{T}}-\nabla\hat{\Omega}+\mathbf{T}_s)\,dV=-\int_{\partial V_e}\nabla\varphi_k\cdot\hat{\mathbf{e}}\,dS,\quad\forall\varphi_k. \tag{41}$$

Equations (38)–(39) and (40)–(41) correspond to the Galerkin formulations

$$\int_V\left\{\nabla\times\mathbf{N}_k\cdot\mu^{-1}\nabla\times\mathbf{A}+\mathbf{N}_k\cdot\sigma\frac{\partial}{\partial t}(\mathbf{A}+\nabla\phi)\right\}dV=\int_V\mathbf{N}_k\cdot\mathbf{J}_s\,dV+\int_{\partial V_h}\mathbf{N}_k\cdot\mathbf{h}\,dS,\quad\forall\mathbf{N}_k \tag{42}$$

$$\int_V\nabla\varphi_k\cdot\sigma\frac{\partial}{\partial t}(\mathbf{A}+\nabla\phi)\,dV=\int_V\nabla\varphi_k\cdot\mathbf{J}_s\,dV+\int_{\partial V_h}\nabla\varphi_k\cdot\mathbf{h}\,dS,\quad\forall\varphi_k \tag{43}$$

and

$$\int_V\left\{\nabla\times\mathbf{N}_k\cdot\sigma^{-1}\nabla\times\mathbf{T}+\mathbf{N}_k\cdot\frac{\partial}{\partial t}[\mu(\mathbf{T}-\nabla\Omega+\mathbf{T}_s)]\right\}dV=-\int_{\partial V_e}\mathbf{N}_k\cdot\mathbf{e}\,dS,\quad\forall\mathbf{N}_k \tag{44}$$

$$\int_V -\nabla\varphi_k \cdot \frac{\partial}{\partial t}\left[\mu(\mathbf{T}-\nabla\Omega+\mathbf{T}_s)\right] dV$$

$$= -\int_{\partial V_c} \nabla\varphi_k \cdot \mathbf{e}\, dS, \quad \forall\varphi_k \tag{45}$$

in the time domain.

Like in the magnetostatic case, a visualisation of the local error density distribution can be obtained by reporting the cloud of pairs ($\mathbf{B}=\nabla\times\mathbf{A}$, $\mathbf{H}=\mathbf{T}-\nabla\Omega+\mathbf{T}_s$) and ($\mathbf{J}=\nabla\times\mathbf{T}+\mathbf{J}_s$, $\mathbf{E}=-\partial\mathbf{A}/\partial t-\nabla\,\partial\phi/\partial t$) in comparison with the curves representing the constitutive equations. Both local and global errors can also be calculated, because both ($\mathbf{E}$, $\mathbf{B}$) and ($\mathbf{J}$, $\mathbf{H}$) are available in the same mesh. Also in the eddy current case, the local error distributions offer a clear indication for mesh refinement.

In addition, there is the possibility of having bounds for functionals (36)–(37), according to the inequalities (holding for p real and positive)

$$\Xi(\hat{\mathbf{A}}+\nabla\hat{\phi},\, p) \geqslant \Xi\left(-\frac{\hat{\mathbf{E}}_0}{p},\, p\right) = -\Theta(\hat{\mathbf{H}}_0-\hat{\mathbf{T}}_s,\, p)$$

$$\geqslant -\Theta(\hat{\mathbf{T}}-\nabla\hat{\Omega},\, \bar{p}) \quad \forall\hat{\mathbf{A}},\, \hat{\phi},\, \hat{\mathbf{T}},\, \hat{\Omega},\, p. \tag{46}$$

The simplifying assumptions made at the beginning of this section can readily be removed.

If $V_c \neq V$ it is sufficient to enforce $\nabla\times\mathbf{T}=\mathbf{0}$ exactly in the region $V-V_c$, where $\sigma=0$ (a possible choice is $\mathbf{T}=\mathbf{0}$ if $V-V_c$ is simply connected). In this way, λ_e is automatically zero in $V-V_c$ and hence the global functional (30) becomes

$$\Lambda(\hat{\mathbf{A}}+\nabla\hat{\phi},\, \hat{\mathbf{T}}-\nabla\hat{\Omega},\, p)$$

$$= \int_V \lambda_m(\nabla\times\hat{\mathbf{A}},\, \hat{\mathbf{T}}-\nabla\hat{\Omega}+\hat{\mathbf{T}}_s,\, p)\, dV$$

$$+ \int_{V_c} \lambda_e(\nabla\times\hat{\mathbf{T}}+\hat{\mathbf{J}}_s,\, -p\hat{\mathbf{A}}-p\,\nabla\hat{\phi},\, p)\, dV, \tag{47}$$

where it is clear that the scalar potential ϕ plays a role only inside V_c.

The treatment of nonzero initial conditions is described in the Appendix, where all the key features of the approach are highlighted with the help of a circuit analogue.

EXAMPLES

Both formulations have been applied to the calculation of the electromagnetic field given by a uniform source current $\mathbf{J}_s$ in a cube of 1 m^3.

In Fig. 2 we show the $B-H$ plot relative to the numerical solution of the nonlinear magnetostatic problem in which the current density $\mathbf{J}_s=0.1$ MA/m^2 is parallel to a side of the cube, with the homogeneous boundary condition $\mathbf{B}\cdot\mathbf{n}=0$.

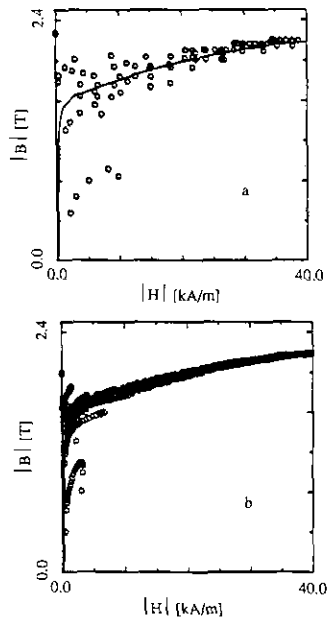

FIG. 2. $B-H$ plots (pairs at the Gauss points) relative to the numerical solutions of a nonlinear magnetostatic problem in a cube in comparison with the magnetic characteristic: (a) discretization of $\frac{1}{8}$ of the cube into $5\times5\times1$ hexahedral elements, with $\Theta=8\times3753.98\,J$ and $-\Xi=8\times3652.40\,J$; (b) $20\times20\times1$ discretization with $\Theta=8\times3727.61\,J$ and $-\Xi=8\times3718.83\,J$.

In Fig. 3 we show the $B-H$ and $J-E$ plots relative to the numerical solution of the linear eddy current problem in which a step of $\mathbf{J}_s=10$ MA/m^2, parallel to a side of the cube, is applied. The resistivity is $1/\sigma=1\mu\Omega m$ and the homogeneous boundary condition $\mathbf{E}\times\mathbf{n}=\mathbf{0}$ is applied. Table I reports the values of Ξ and Θ for several values of p.

These results show how the local and global constitutive errors are reduced by a mesh refinement and are in a good agreement with the analytical solutions. One may wonder why in Fig. 2 and 3 the points are distributed both above and under the curves representing the constitutive equa-

TABLE I

Values in MJ (Referred to the Whole Domain) of Θ, Ξ, and Λ Given by the Numerical Results Illustrated in Fig. 3

	$5\times5\times1$			$20\times20\times1$		
p	$-p^2\Xi$	$p^2\Theta$	$p^2\Lambda$	$-p^2\Xi$	$p^2\Theta$	$p^2\Lambda$
10^{-2}	1.92	2.24	0.32	1.96	2.37	0.41
10^{-1}	22.99	23.45	0.46	23.33	23.45	0.12
1	216.70	221.11	4.41	219.69	220.16	0.47
10	1458.00	1483.24	25.24	1471.33	1474.81	3.48
10^2	4987.17	4994.00	6.83	4987.34	4993.82	6.48

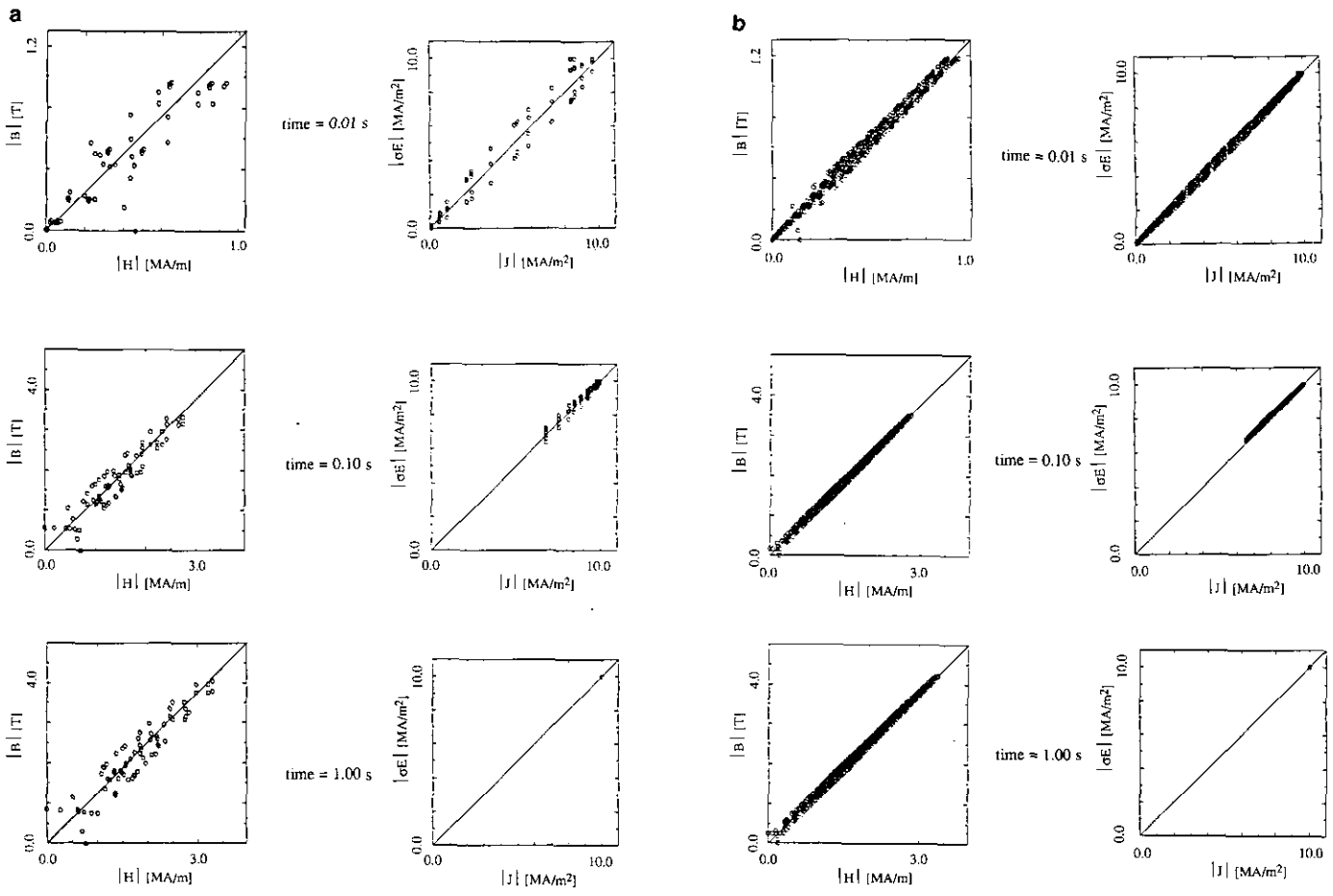

FIG. 3. $B-H$ and $J-E$ plots (pairs at the Gauss points) relative to the numerical solutions of a linear eddy current problem in a cube ($\mu=\mu_0$) at various times: (a) $5\times5\times1$ discretization; (b) $20\times20\times1$ discretization.

tions. This can be explained by noting that if all the points were, for instance, under the $B-H$ curve, then it would be possible to reduce the constitutive error by multiplying **A** everywhere by a constant factor slightly larger than unity (this would be possible since in both examples $\mathbf{A}\times\mathbf{n}=\mathbf{0}$ on the boundary).

Furthermore, in the linear problem of Fig. 3, along certain lines (normal to the faces) **B** is piecewise constant, whereas $\mu_0\mathbf{H}$ is piecewise linear with interelement continuity. It is apparent that the constitutive error is not minimized if the two curves do not intersect each other.

We have also analysed the TEAM Workshop problem 10 [25] which concerns the calculation of the electromagnetic field produced by a coil of rectangular cross-section in the presence of a magnetic circuit made up of thin iron plates and small air gaps. Here we report some results concerning the magnetostatic field configuration achieved when all the transients have estinguished.

Figure 4 shows the magnetic field in the iron plates,

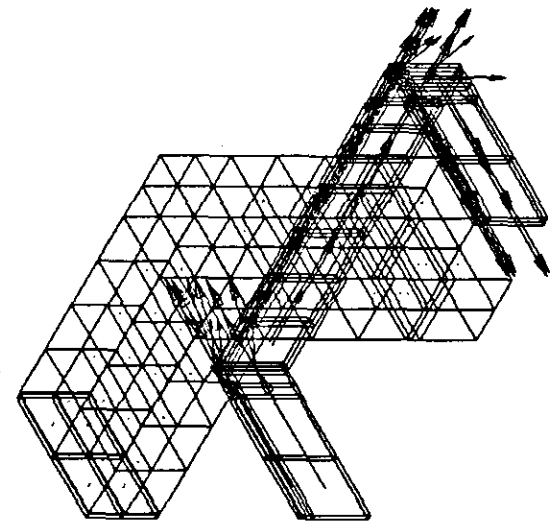

FIG. 4. TEAM Workshop problem 10: magnetic field in the iron after termination of transients.

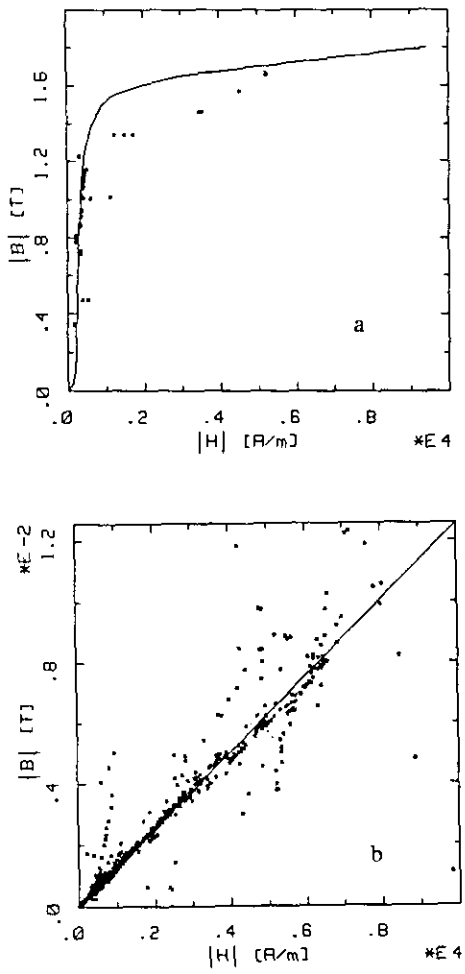

FIG. 5. TEAM Workshop problem 10: $B-H$ plots (pairs at the element centroids) related to the iron (a) and air (b) region after termination of transients.

whereas Fig. 5 shows the B-H plots. In this case, the values of the two functionals are $\Xi = -25.6$ mJ, $\Theta = 31.4$ mJ. The comparison [26] with the experimental results [25], in terms of average flux densities at three specified cross sections, shows that the numerical error is mainly due to the bad behavior of the $\mathbf{T}, \Omega$ solution (the mesh is rather coarse and there is a single layer of elements in the air gap). In fact, despite the poor results given by the $\mathbf{T}, \Omega$ solution (the relative errors on the three flux densities are 3.0, 10.8, and 6.8%), the $\mathbf{A}, \phi$ solution is in excellent agreement with the measured values (with relative errors of 0.5, 0.3, and 0.9%, respectively).

CONCLUSIONS

In this paper, some aspects of the numerical computation of static and low frequency electromagnetic fields have been reviewed. In particular, the formulations discussed here are based on the use of edge elements. These elements allow for the efficient introduction of a gauge directly applied on the shape functions, minimizing the number of unknowns in terms of vector potentials. The features of these elements are related to the possibility of representing vector fields whose tangential components are constrained to be everywhere continuous, while allowing for possible discontinuities of the normal component across adjacent elements. These advantages are in part counterbalanced by the impossibility of representing a field whose curl is uniform in a distorted hexahedral edge element. In fact, in this case, the flux ($\int \nabla \times \mathbf{A} \cdot \mathbf{n}\, dS$ or $\int \nabla \times \mathbf{T} \cdot \mathbf{n}\, dS$) is kept uniform in the master element, so that the curl in the distorted element (whose opposite faces are not parallel) varies according to the inverse of the Jacobian.

Another important point is related to the discussion of the properties of the dual electric ($\mathbf{A}, \phi$) and magnetic ($\mathbf{T}, \Omega$) formulations. Following the theory described in [1], in the magnetostatic case, the constitutive error-based approach leads to upper and lower bounds for energy related functionals.

In the frequency domain some authors [3–5], adopting a different approach, seem to arrive at the definition of upper and lower bounds for the approximate solutions obtained using numerical procedures. However, the error-based approach does not yield analogous general results when applied to transient or steady state electomagnetic field problems [2]. Here we have shown that the particular determination of the Laplace transform on the real axis is able to produce real bounding functionals.

It is possible to envisage dual problemss in which σ and μ play dual roles. In such cases electric and magnetic formulations provide exactly the same numerical results for dual quantities. So, neither formulation is definitely better than the other one, and the choice of the method might be made according to the particular problem and objectives (e.g., connectivity of the conducting region, precision, or solenoidality of the approximate field solutions).

However, our point of view is that both computations should be performed whenever possible. In fact, the final point highlighted in this paper is the definition of the local constitutive error, which represents one of the most reliable ways of establishing: (i) how good is the numerical solution; (ii) a valuable criterium for mesh refinement; (iii) a powerful means for the identification of input data errors (especially when numerical procedures are employed by nonexpert users). Work is now in progress to extend the error-based edge element formulations to nonlinear cases [27] and wave propagation [28].

APPENDIX

In this appendix, the basic features of the methods illustrated in the paper will be highlighted with reference to

the simple electric network shown in Fig. A1. In the computational method for the eddy current problem described in the paper, the primitive variables are the potentials instead of the fields in order to automatically verify Maxwell equations. Similarly, for the network analysis we will assume adequate unknowns to automatically verify Kirchhoff laws, namely loop currents and time integrals of the node potentials (node fluxes). Thus, grounding node B and selecting the loop currents shown in Fig. A1, the independent variables become $\varphi(t)$ and $i(t)$.

The solution of the problem will then be provided by the functions $\varphi(t)$ and $i(t)$ which verify constitutive equations and the initial condition:

$$\varphi = L(i + i_e) \tag{A1}$$

$$i = G\, d\varphi/dt \tag{A2}$$

$$\varphi(0) = \varphi_0. \tag{A3}$$

These equations are in close relationship with (6), (7), (26), (27). Thus, similar to the field treatment, we can define

$$\lambda_L(\varphi, i) = [\varphi - L(i + i_e)]^2/2L \tag{A4}$$

$$\lambda_G(\varphi, i) = [i - G\, d\phi/dt]^2/2G \tag{A5}$$

and

$$\Lambda_L(\hat{\varphi}, \hat{\imath}, p) = [\hat{\varphi} - L(\hat{\imath} + \hat{\imath}_e)]^2/2L \tag{A6}$$

$$\Lambda_G(\hat{\varphi}, \hat{\imath}, p) = [\hat{\imath} - G(p\hat{\varphi} - \varphi_0)]^2/2G, \tag{A7}$$

where $\hat{a}(p)$ denotes Laplace transform of $a(t)$.

The sum $\Lambda = \Lambda_G + \Lambda_L$ can also be expressed as

$$\Lambda = \Xi + \Theta, \tag{A8}$$

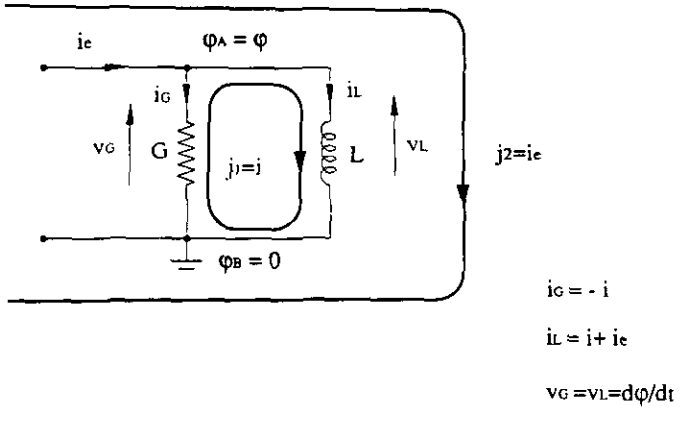

FIG. A1. Electric network used in the circuit analogy: $L = 1H$, $G = 1\Omega^{-1}$, $i_e = 1A$, $\varphi_0 = 0$.

where

$$\Xi(\hat{\varphi}, p) = \frac{\hat{\varphi}^2}{2L} + \frac{G}{2p}(p\hat{\varphi} - \varphi_0)^2 - \hat{\varphi}\hat{\imath}_e \tag{A9}$$

$$\Theta(\hat{\imath}, p) = \tfrac{1}{2} L(\hat{\imath} + \hat{\imath}_e)^2 + \frac{\hat{\imath}^2}{2pG} - \frac{\varphi_0}{p}\hat{\imath}. \tag{A10}$$

The stationary points of Ξ and Θ (as well as their minimization for real positive values of p) are given by:

$$\frac{\hat{\varphi}}{L} + G(p\hat{\varphi} - \varphi_0) - \hat{\imath}_e = 0 \tag{A11}$$

$$L(\hat{\imath} + \hat{\imath}_e) + \frac{\hat{\imath}}{pG} - \frac{\varphi_0}{p} = 0 \tag{A12}$$

which are the Kirchhoff laws written in the Laplace domain.

Fig. A2 shows the plot of $p^2\Xi$, $p^2\Theta$, and $p^2\Lambda$ obtained solving Eqs. (A11) and (A12) in the time domain by Crank–Nicholson scheme. It can be noted that the error peak is localized around $p = 1/\Delta t$, where Δt is the time step of Crank–Nicholson integration.

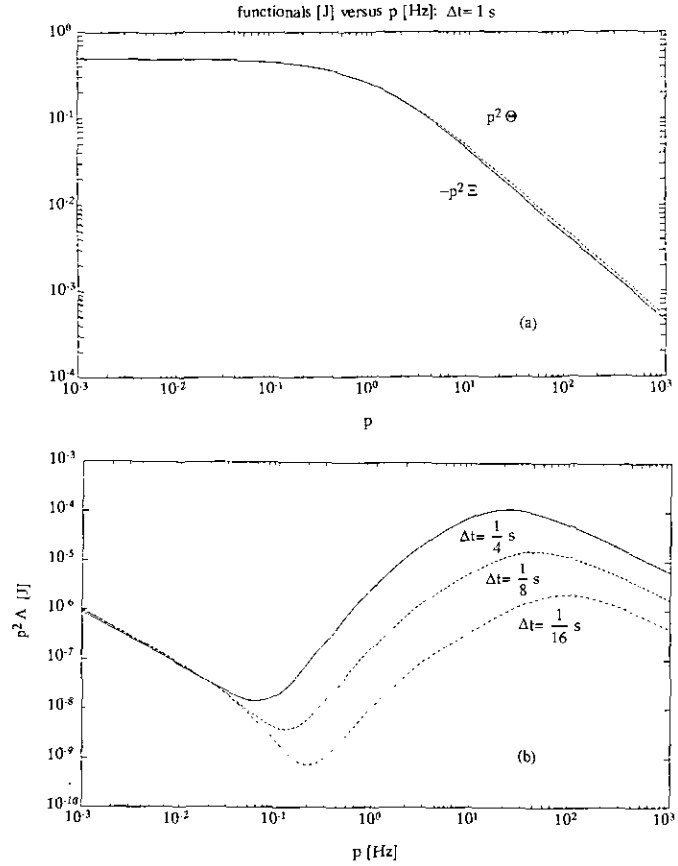

FIG. A2. Plots of $p^2\Xi$, $p^2\Theta$ and $p^2\Lambda$ associated with the solutions of Eqs. (A11) and (A12) obtained in the time domain by Cranck-Nicholson scheme using various time steps.

ACKNOWLEDGMENTS

This paper is mainly based on an invited talk presented at the 4th International IGTE Symposium held in Graz, Austria, 10–12 October 1990. This work is dedicated to the memory of Jafar A. H. Rikabi.

REFERENCES

1. J. Rikabi, C. F. Bryant and E. M. Freeman, *Int. J. Num. Methods Eng.* **26**, 1963 (1988).
2. J. Rikabi, C. F. Bryant, and E. M. Freeman, *IEE Proc., Pt. A* **135**, 208 (1988).
3. P. Hammond and J. Penman, *IEE Proc.* **125**, 701 (1978).
4. P. Hammond, *IEE Proc., Pt. A* **136**, 207 (1989).
5. P. Yang and D. Zhu, in *Proceedings of Beijing International Symposium on Electromagnetic Fields in Electrical Engineering (BISEF'88)* (IAP, Pergamon, Elmsford, NY, 1989), p. 354.
6. R. Albanese and G. Rubinacci, *IEEE Trans. Magn.* **MAG-24**, 98 (1988).
7. R. Albanese and G. Rubinacci, *IEE Proc., Pt. A* **135**, 457 (1988).
8. R. Albanese and G. Rubinacci, *Int. J. Num. Methods Eng.* **29**, 515 (1990).
9. J. C. Nedelec, *Numer. Math.* **35**, 315 (1980).
10. A. Bossavit, *IEEE Trans. Magn.* **MAG-24**, 74 (1988).
11. G. Mur and A. T. De Hoop, *IEEE Trans. Magn.* **MAG-21**, 2188 (1985).
12. J. S. van Welij, *IEEE Trans. Magn.* **MAG-21**, 2239 (1985).
13. Z. Ren and J. C. Verité, in *Proceedings, Beijing International Symposium on Electromagnetic Fields in Electrical Engineering (BISEF'88)* (IAP, Pergamon, Elmsford, NY, 1989), p. 596.
14. A. Kameari, *IEEE Trans. Magn.* **MAG-26**, 466 (1990).
15. A. Bossavit and J. C. Verité, *IEEE Trans., Magn.* **MAG-18**, 431 (1982).
16. Z. Ren, F. Bouillault, A. Razek, A. Bossavit, and J. C. Verité, *IEEE Trans. Magn.* **MAG-26**, 470 (1990).
17. O. Biro and K. Preis, *IEEE Trans. Magn.* **MAG-25**, 3145 (1989).
18. C. F. Bryant, C. R. I. Emson, and C. W. Trowbridge, *IEEE Trans. Magn.* **MAG-26**, 430 (1990).
19. R. Albanese and G. Rubinacci, *IEE Proc., Pt. A* **137**, 16 (1990).
20. C. J. Carpenter, *IEE Proc.* **124**, 1026 (1977).
21. M. L. Brown, *IEE Proc. Pt. A* **129**, 46 (1982).
22. R. Albanese, R. Martone, G. Miano, and G. Rubinacci, *IEEE Trans. Magn.* **MAG-21**, 2299 (1985).
23. A. Kameari, *J. Comput. Phys.* **42**, 124 (1981).
24. R. Albanese and G. Rubinacci, *IEEE Trans. Magn.* **MAG-26**, 650 (1990).
25. T. Nakata, M. Nakano, K. Fujiwara, and T. Kanada, *An. Fis. Ser. B* **86**, 190 (1990).
26. R. Albanese *et al.* (Eds.), *Proceedings, Third International TEAM Workshop, Sorrento, Italy, 12–13 July 1991* (Commission of the European Communities, 1992), EUR 14173EN.
27. R. Albanese, E. Coccorese, R. Martone, G. Miano, and G. Rubinacci, *IEEE Trans. Magn.* **MAG-27**, 3990 (1991).
28. R. Albanese and G. Rubinacci, *Rev. Roum. Sci. Tech. Ser. Electrotech. Energ.*, submitted.